Металлофиз. новейшие технол. / Metallofiz. Noveishie Tekhnol.
2014, т. 36, № 3, сс. 419–429
Оттиски доступны непосредственно от издателя
Фотокопирование разрешено только
в соответствии с лицензией

ЭЛЕКТРОННЫЕ СТРУКТУРА И СВОЙСТВА

PACS numbers: 63.20.dk, 71.15.-m, 71.15.Mb, 71.38.-k, 72.10.Di, 72.15.Eb

Interaction between Electron and Phonon Subsystems in Hafnium Diboride

S. M. Sichkar

G. V. Kurdyumov Institute for Metal Physics, N.A.S. of Ukraine,
36 Academician Vernadsky Blvd.,
UA-03680 Kyyiv-142, Ukraine

Ab initio calculation of the electron–phonon coupling functions is carried out, using full potential LMTO method. Low value of the averaged electron–phonon interaction constant for HfB_2 $\lambda = 0.17$ indicates that there is no evidence of superconductivity in this compound. Electrical resistivity and anisotropy factor $\rho_z/\rho_x = 1.079$ ($T = 300$ K) are theoretically calculated. A good agreement with experimental data of electrical resistivity is achieved. Comparative analysis of ABINIT, SIESTA, VASP, and present LMTO method for phonon spectra calculating is performed.

Ab initio розрахунок функцій електрон-фононного зв'язку виконано за методом ЛМТО з використанням повного потенціалу. Низьке значення усередненої константи електрон-фононної взаємодії для HfB_2 $\lambda = 0{,}17$ свідчить, що немає підстав для виникнення надпровідного стану в цій сполуці. Вперше було розраховано електричний опір і коефіцієнт анізотропії $\rho_z/\rho_x = 1{,}079$ ($T = 300$ К) для дибориду гафнію. Було досягнуто добру узгодженість з експериментальними даними для електричного опору. У роботі виконано порівняльний аналіз результатів розрахунків фононних спектрів методами ABINIT, SIESTA, VASP та запропонованим методом ЛМТО з детальним обговоренням одержаних відмінностей.

Ab initio расчёт функций электрон-фононной связи выполнен в рамках метода ЛМТО с использованием полного потенциала. Низкое значение усреднённой константы электрон-фононного взаимодействия для HfB_2 $\lambda = 0{,}17$ свидетельствует, что нет оснований для возникновения сверхпроводящего состояния в этом соединении. Впервые были рассчитаны электрическое сопротивление и коэффициент анизотропии $\rho_z/\rho_x = 1{,}079$ ($T = 300$ К) для диборида гафния. Было достигнуто хорошее согласие с экспериментальными данными для электрического сопротивления. В работе выполнен сравнительный анализ результатов расчётов фононных спектров методами ABINIT, Siesta, VASP и предложенным методом ЛМТО с детальным обсуждением полученных различий.

Key words: lattice dynamics, electron–phonon interaction, phonon spectrum, thermodynamic properties, electrical resistivity, diborides.

(Received 18 November, 2013)

1. INTRODUCTION

With its high thermodynamic stability, hardness, conductivity, corrosion resistance, and significant melting point, ceramics based on transition metal borides is attractive material for practical application in various fields of engineering, metallurgy, instrumentation, chemical industry, *etc*. Hafnium boride (melting point 3250°C, microhardness $\cong 29 \pm 5$ GPa) is used as an extremely wear-resistant coating and for production of superhard alloys. In addition, HfB_2 is one of the most refractory compounds and is used for the production of rocket jets and some structural elements of gaseous nuclear rocket engines.

The opening of a critical transition $T_c \cong 40$ K in MgB_2 [1] and creation of new superconducting materials based on it (in the form of films, ceramics, long wires and tapes) stimulated the development of work on a detailed study of superconductivity in other diborides. Unfortunately, according to Ref. [2], no superconducting transition down to 0.42 K has been observed in powders of diborides of transition metals (M) MB_2 (M = Ti, Zr, V, Ta, Cr, Mo, U). Only NbB_2 is expected to be a superconductor with a rather low transition temperature (< 1 K). On the other hand, two experimental results (superconductivity up to $T_c = 9.5$ K in TaB_2 according to Ref. [2] and $T_c = 7$ K in ZrB_2 [3]) hold out hope to find superconducting materials based on metal diborides.

Presently, a number of experimental studies exists dealing with the physical properties of HfB_2, such as thermal and electrical properties [4–7], mechanical [8], and elastic properties [9].

Lawson *et al.* [10] studies the electronic structure and lattice properties of HfB_2 in a frame of the density functional theory (DFT). Lattice constants and elastic constants are determined. Computations of the electronic density of states, band structure, electron localization function, *etc*., show the diverse bonding types that exist in these materials. They also suggest the connection between the electronic structure and the superior mechanical properties. Lattice dynamical effects are considered, including phonon dispersions, vibrational densities of states, and specific heat curves. The bonding nature, elastic property and hardness are investigated by Zhang *et al.* [11] for HfB_2 using the first principles total-energy plane-wave pseudopotential (PW–PP) method. They also reported the elastic anisotropy, Poisson ratio, hardness, and Debye temperature in HfB_2. Deligoz *et al.* [12] investigate the structural parameters (the lattice constants and bond length) and phonon dispersion relations in HfB_2 and TaB_2 compounds using the first-

principles total energy calculations. Zhang *et al.* [13] investigated the ideal tensile and shear strengths of TiB_2, ZrB_2, and HfB_2 by first-principles stress-strain calculations. Due to the nonlinearity of the stress response at large strains, the plastic anisotropy cannot be derived from elastic constants. Based on the relative stiffness of boron hexagons, a bond length indicator is obtained to characterize the preference for basal or prismatic slip in diborides.

Authors of Ref. [4] determined the thermal conductivity, thermal expansion, Young's modulus, flexural strength, and brittle-plastic deformation transition temperature for HfB_2 as well as for $HfC_{0.98}$, $HfC_{0.76}$, and $HfN_{0.92}$ ceramics. The thermal conductivity of HfB_2 exceeds that of the other materials by a factor of 5 at room temperature and by a factor of 2.5 at 820°C. Pure HfB_2 has a strength of 340 MPa in 4 point bending, which is constant from room temperature to 1600°C, while a $HfB_2 + 10\%$ HfC_x has a higher room temperature bend strength of 440 MPa, but it drops to 200 MPa at 1600°C. The results of the theoretical modelling suggest that HfB_2 should survive the high thermal stresses generated during the nozzle test primarily because of its superior thermal conductivity. Yang *et al.* [14] used *in situ* spectroscopic ellipsometry to analyse HfB_2 thin films. Modelling the film optical constants with a Drude–Lorentz model, the film thickness, surface roughness, and electrical resistivity are measured. Modelling the real-time data in terms of film thickness and surface roughness, the film nucleation and growth morphology are determined as a function of substrate type, substrate temperature, and precursor pressure. Zhang *et al.* [6] experimentally investigated the thermal and electrical transport properties of various spark plasma-sintered HfB_2 based polycrystalline ceramics over the 298–700 K temperature range. Measurements of thermal diffusivity, electrical resistivity, and Hall coefficient are reported, as well as the derived properties of thermal conductivity, charge carrier density, and charge carrier mobility. The thermal conductivity decreases with increasing temperature.

Despite a lot of publications, there are still many open questions related to the physical properties of HfB_2 diboride. In recent years, the most theoretical efforts were devoted to the lattice and mechanical properties of HfB_2. However, up to now there is no theoretical explanation of the electron–phonon interaction and anisotropy of the electrical resistivity in HfB_2. The aim of a given work is a complex investigation of the phonon spectra, Eliashberg electron–phonon and transport spectral functions, temperature dependence, and anisotropy of electrical resistivity of the HfB_2 diboride. The paper is organized as follows. Section 2 presents the details of the calculations. Section 3 is devoted to the phonon spectra, electron–phonon interaction, and electrical resistivity in HfB_2. The results are compared with available experimental data. Finally, the results are summarized in Sec. 4.

2. COMPUTATIONAL DETAILS

Most known transition-metal diborides MB_2 are formed by transition elements of III–VI group (Sc, Ti, Zr, Hf, V, Nb, and others) and have a layered hexagonal $C32$ structure of the AlB_2-type with the space group symmetry $P6/mmm$ (number 191). By choosing appropriate primitive lattice vectors, the atoms are positioned at Hf (0, 0, 0), B (1/3, 1/6, 1/2), and B (2/3, 1/3, 1/2) in the unit cell. The distance between Hf–Hf is equal to c. Actually, this structure is quite close packed, and can be coped efficiently and accurately by the atomic sphere approximation method. However, for precise calculation of the phonon spectra and electron–phonon interaction, full potential approximation should be used.

The Eliashberg function (the spectral function of the electron–phonon interaction) expressed in terms of the phonon linewidths $\gamma_{\mathbf{q}\nu}$ has the form [15]

$$\alpha^2 F(\omega) = \frac{1}{2\pi N(\varepsilon_F)} \sum_{\mathbf{q}\nu} \frac{\gamma_{\mathbf{q}\nu}}{\omega_{\mathbf{q}\nu}} \delta(\omega - \omega_{\mathbf{q}\nu}). \quad (1)$$

The linewidths characterize the partial contribution of each phonon:

$$\gamma_{\mathbf{q}\nu} = 2\pi\omega_{\mathbf{q}\nu} \sum_{\mathbf{k}jj'} \left| g^{\mathbf{q}\nu}_{\mathbf{k}+\mathbf{q}j',\mathbf{k}j} \right|^2 \delta(\varepsilon_{\mathbf{k}j} - \varepsilon_F) \delta(\varepsilon_{\mathbf{k}+\mathbf{q}j'} - \varepsilon_F), \quad (2)$$

$N(\varepsilon_F)$ is the electron density of states per atom and per spin on the Fermi level ε_F , and $g^{\mathbf{q}\nu}_{\mathbf{k}+\mathbf{q}j',\mathbf{k}j}$ is the electron–phonon interaction matrix element.

The electron–phonon interaction constant is defined as:

$$\lambda = 2\int \alpha^2 F(\omega)\omega^{-1} d\omega. \quad (3)$$

It can also be expressed in terms of the phonons linewidths:

$$\lambda = \sum_{\mathbf{q}\nu} \frac{\gamma_{\mathbf{q}\nu}}{\pi N(\varepsilon_F)\omega^2_{\mathbf{q}\nu}}, \quad (4)$$

The double summation over Fermi surface in Eq. (2) is carried out on dense mesh (793 point in the irreducible part of the Brillouin zone (BZ)).

For the calculation of the phonon spectra and electron–phonon interaction, a scalar relativistic FP-LMTO method [16] is used. In these calculations, author used the Perdew–Wang [17] parameterization of the exchange-correlation potential in general gradient approximation. BZ integrations are performed using the improved tetrahedron method [18]. Phonon spectra and electron–phonon matrix elements are calculated for 50 points in the irreducible part of the BZ, using the linear

response scheme [16].

The 5*s*- and 5*p*-semi-core states of HfB_2 are treated as valence states in separate energy windows. Variations in charge density and potential are expanded in spherical harmonics inside the MT-sphere as well as in 2894 plane waves in the interstitial area with 88.57 Ry cut-off energy for HfB_2. As for the area inside the MT-spheres, 3**k**–*spd* LMTO basis set energy (–0.1, –1, –2.5 Ry) is used with one-centre expansions inside the MT-spheres performed up to $l_{max} = 6$. Calculations are performed with the experimentally observed lattice constants: $a = 3.141$ Å and $c = 3.47$ Å for HfB_2 [19].

3. RESULTS AND DISCUSSION

3.1. Phonon Spectra

The unit cell of HfB_2 contains three atoms, which gives in general case nine phonon branches. Figure 1 shows theoretically calculated phonon density of state for HfB_2 (full curve). The DOS for HfB_2 can be separated into three distinct regions. Based on the author's analysis of relative directions of eigenvectors for each atom in unit cell, it was shown that the first region (with a peak in phonon DOS at 5.2 THz) is dominated by the motion of Hf. This region belongs to the acoustic phonon

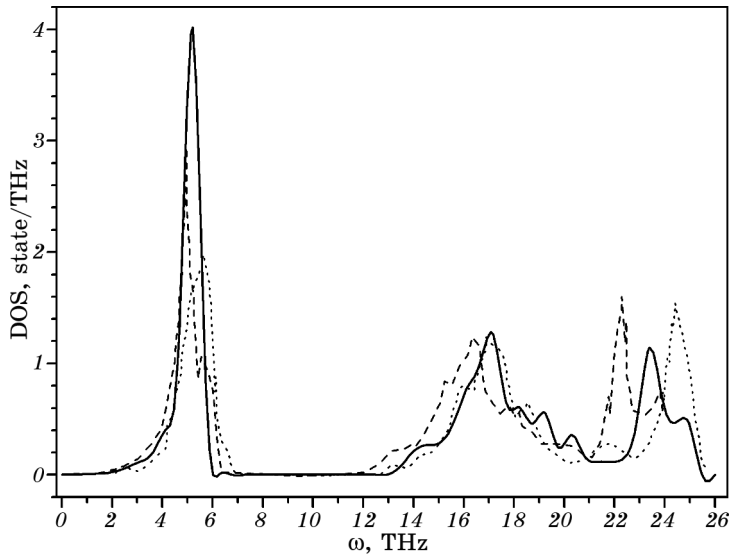

Fig. 1. Theoretically calculated phonon density of states (full line) $F(\omega)$ for HfB_2. The dotted and dashed lines present the calculated phonon DOS of HfB_2 by Deligoz *et al.* [12] and Lawson *et al.* [10], respectively.

modes. The second wide region (14–20 THz) results from the coupled motion of Hf and two B atoms in the unit cell. The E_{1u}, A_{2g}, B_{1g} phonon modes (see Table) lie in this area. The phonon DOS in the third region extends from 22 THz to 26 THz. This is caused by the movement of boron atoms and is expected since boron is lighter than Hf. The covalent character of the B–B bonding is also crucial for the high frequency of phonons. The in-plane E_{2g} mode belongs to this region. The second and third regions represent optical phonon modes in crystals. The most significant feature in the phonon DOS is a gap around 6–13 THz. This gap is a consequence of the large mass difference between B (10.8 a.u.) and Hf (178.49 a.u.), which leads to decoupling of the transition metal and boron vibrations.

Currently, there are no data concerning the experimentally measured phonon DOS in HfB_2. So, author compares his results with theoretically calculated phonon DOS by Deligoz *et al.* [12] and Lawson *et al.* [10] (see Fig. 1 and Table). Calculations of Deligoz *et al.* [12] are based on the density functional formalism and generalized gradient approximation.

They used the Perdew–Burke–Ernzerhof functional [20] for the exchange-correlation energy as it is implemented in the SIESTA code [21]. This code calculates the total energies and atomic Hellmann–Feynman forces using a linear combination of atomic orbitals as the basis set. The basis set consists of finite range pseudoatomic orbitals of the Sankey–Niklewsky type [22], generalized to include multiplexing decays.

The interactions between electrons and core ions are simulated with the separable Troullier–Martins [23] normconserving pseudopotentials. In other words, they used the so-called 'frozen phonon' technique and built an optimized rhombohedral supercell with 36 atoms. This method is inconvenient for calculating phonon spectra for small **q**-points as well as for compounds with large number of atoms per unit cell. Lawson *et al.* [10] used two different codes to calculate the phonon spectra. VASP, the supercell method, based on the projected augmented wave potentials. Second method, ABINIT, uses Fritz Haber Insti-

TABLE. Theoretically calculated phonon frequencies (in THz) in the Γ symmetry point for HfB_2 and calculated phonon frequencies by Deligoz *et al.* Ref. [12] and Lawson *et al.* Ref. [10].

Reference	E_{1u}	A_{2g}	B_{1g}	E_{2g}
Present work	13.76	15.03	17.12	25.17
SIESTA [12]	14.10	15.19	15.87	24.49
VASP [10]	13.34	14.00	16.40	24.16
ABINIT [10]	12.92	13.85	16.01	23.59

tute pseudopotentials in the Troulliers–Martin form. VASP results of Lawson *et al.* [10] is slightly closer to our calculation with respect to ABINIT data. There is a good agreement between author's calculations and the results of Deligoz *et al.* [12] in a shape and energy position of the second peak in the phonon DOS. There is an energy shift towards smaller energies of the first, second and third peaks of the Lawson *et al.* [10] calculations in comparison with the Deligoz *et al.* [12] data. The difference between third peaks in VASP and SIESTA data reaches 2.2 THz. Results presented here lie between these two calculations.

In next section, it will be shown how the shift of the third peak of matrix element at 2.1 THz with respect to the third peak of phonon DOS can dramatically decrease value of averaged electron–phonon coupling. So, SIESTA and VASP codes do not provide phonon spectra with sufficient accuracy for precise calculation of critical superconductivity temperature.

3.2. Electron–Phonon Interaction

Figure 2 shows theoretically calculated Eliashberg functions for HfB_2 as well as electron–phonon prefactor $\alpha^2(\omega)$ (definition of this function is merely ratio $(\alpha^2(\omega)F(\omega)/F(\omega))$); $\alpha^2(\omega)$ has strongly varying character. Therefore, matrix element of electron–phonon interaction cannot be presented in form $\alpha^2(\omega) \approx \text{const}$ and hence well-known McMillan ap-

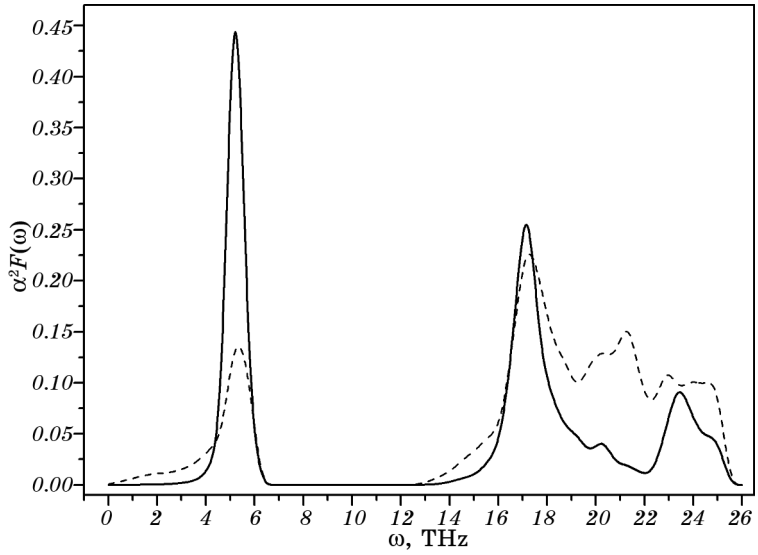

Fig. 2. Theoretically calculated Eliashberg function $\alpha^2F(\omega)$ of HfB_2 (full line) and electron–phonon prefactor $\alpha^2(\omega)$ (dashed line).

proximation [24] is not valid for HfB_2. The electron–phonon coupling cannot be factorized into independent electronic and phonon parts.

There is no difference between main peaks positions of phonon spectra and electron–phonon coupling function. Electron–phonon prefactor has three peaks: 5.2 THz, 17.1 THz, and 21.3 THz (the corresponding peaks in the phonon DOS and Eliashberg function are situated at the 5.2 THz, 17.1 THz, and 23.4 THz frequencies). The difference in the positions of the third peaks in electron–phonon prefactor and in phonon DOS can explain the suppression of high-energy peak in Eliashberg function (23.4 THz). The third peak of matrix element of electron–phonon interaction ($\alpha^2(\omega)$) lies between two main peaks of phonon DOS (in region with low phonon DOS). This fact strongly influences on the decreasing of the value of averaged electron–phonon coupling.

By integrating the Eliashberg function according to Formula (3), the averaged electron–phonon constant is calculated, $\lambda = 0.17$. The constant of the electron–phonon interaction also can be roughly estimated by comparison of the theoretically calculated DOS at the Fermi level and the electron specific heat coefficient γ. $C_p = \gamma T$, where $\gamma = 1.0$ $mJ \cdot mole^{-1} \cdot K^{-2}$ for HfB_2 [25]. HfB_2 possesses quite small value of the DOS at the Fermi level of 0.4 states/(cell·eV). It gives the theoretically calculated $\gamma_b = 0.8$ $mJ \cdot mole^{-1} \cdot K^{-2}$ and $\lambda_h = 0.2$ in qualitative agreement with $\lambda = 0.17$.

To calculate the superconductivity transition temperature T_c for HfB_2, McMillan formula modified by Allen–Dynes [26] is used:

$$T_c = \frac{\omega_{log}}{1.2} \exp\left[\frac{1.04(1+\lambda)}{\lambda - \mu^*(1+0.62\lambda)}\right], \tag{5}$$

where ω_{log}—the effective logarithmically averaged phonon frequency, μ^*—the screening Coulomb pseudopotential. As a result, T_c is less than 0.01 K ($\mu^* \cong 0.10$, $\omega_{log} = 459.25$ K).

3.3. Electrical Resistivity

In the pure metals (excluding low-temperature region), the electron–phonon interaction is the dominant factor governing electrical conductivity of the substance. Using the lowest-order variational approximation, the solution for the Boltzmann equation gives the following formula for the temperature dependence of $\rho_I(T)$:

$$\rho_I(T) = \frac{\pi \Omega_{cell} k_B T}{N(\varepsilon_F)\left\langle \upsilon_I^2 \right\rangle} \int_0^\infty \frac{d\omega}{\omega} \frac{\zeta^2}{\sinh^2 \zeta} \alpha_{tr}^2 F(\omega), \tag{6}$$

where the subscript I specifies the direction of the electrical current. In this work, two directions: [0001] (c-axis or z direction) and $[10\bar{1}0]$

(*a*-axis or *x* direction) are investigated; $< \upsilon_I^2 >$ is the average square of the I component of the Fermi velocity, $\zeta = \omega/(2k_B TI)$.

Mathematically, the transport function $\alpha_{tr}^2 F(\omega)$ differs from $\alpha^2 F(\omega)$ only by an additional factor $[1 - \upsilon_I(\mathbf{k})\upsilon_I(\mathbf{k}')/ < \upsilon_I^2 >]$, which preferentially weights the backscattering processes.

Formula (6) remains valid in the range $\Theta_{tr} = 5 < T < 2\Theta_{tr}$ [16], where:

$$\Theta_{tr} \equiv < \omega^2 >_{tr}^{1/2}, \tag{7}$$

$$< \omega^2 >_{tr} = \frac{2}{\lambda_{tr}} \int_0^\infty \omega \alpha_{tr}^2 F(\omega) d\omega, \tag{8}$$

$$\lambda_{tr} = 2 \int_0^\infty \omega^{-1} \alpha_{tr}^2 F(\omega) d\omega. \tag{9}$$

The low-temperature electrical resistivity is the result of electron-electron interaction, size effects, scattering on impurities, *etc.*; however, for high temperatures, it is necessarily to take into account the effects of anharmonicity and the temperature smearing of the Fermi surface. In present calculations, $\Theta_{tr} = 654.4$ K for *c*-axis, and 679.9 K for *a*-axis for HfB_2.

Figure 3 represents the theoretically calculated temperature dependence of electrical resistivity of HfB_2 for the [0001] direction (full curve) and the basal $[10\bar{1}0]$ direction (dashed curve) and experimental

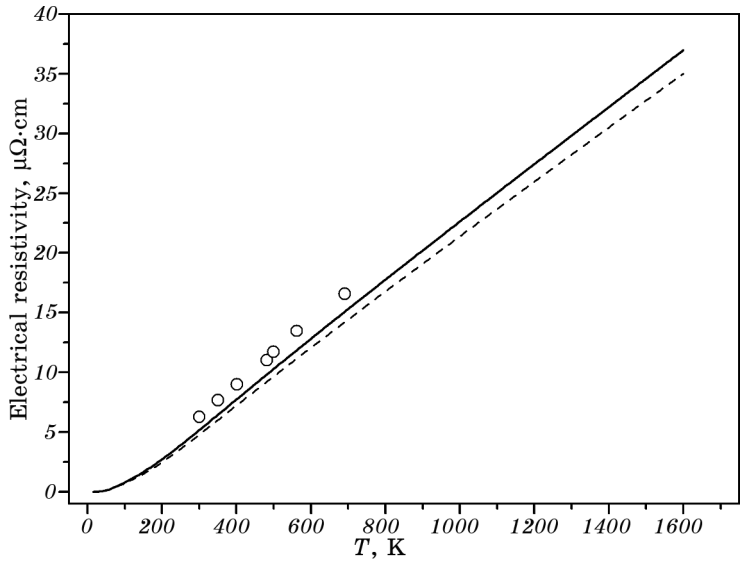

Fig. 3. Theoretically calculated for the [0001] direction (full curve) and the basal $[10\bar{1}0]$ direction (dashed curve), and experimentally measured temperature dependence of electrical resistivity of HfB_2 [6] (open circles).

measurements for polycrystalline HfB_2 [6] (open circles). Specimen of HB_2 ceramics is produced by spark plasma sintering method and has good ratio of experimental and theoretically calculated density $\rho_{exp}/\rho_{th} = 98.1\%$ Theoretical results are in a good agreement with the experiment. The small discrepancy does not exceed accuracy of calculation. Anisotropy ratio of electrical resistivity at $T = 300$ K: $\rho_z/\rho_x = 1.079$. Actually, this fact indicates that for HfB_2 anisotropy is not clearly expressed.

4. SUMMARY

The phonon subsystem as well as the electron–phonon interaction of HfB_2 is studied using full potential linear muffin-tin orbital methods.

The calculated phonon spectra and phonon DOS for HfB_2 show that different theoretical approaches to the calculation may give sufficient discrepancies, especially in high-energy region. Therefore, it is very important to use accurate shape of the crystalline potential in self-consistent calculation.

There are no regions in **k**-space with high electron–phonon interaction or phonon dispersion curves with soft modes in HfB_2. The averaged electron–phonon interaction constant for HfB_2 is rather small $\lambda = 0.17$. This clearly indicates that there is no evidence of superconductivity in this compound. Of course, this conclusion matches to direct calculation of transition temperature according Formula (5).

The temperature dependence of the electrical resistivity in HfB_2 is calculated in the lowest-order variational approximation of the Boltzmann equation. These results are in good agreement with the experiment. Anisotropic behaviour of the electrical resistivity in hafnium diboride is rather small.

REFERENCES

1. J. Nagamatsu, N. Nakagawa, T. Muranaka, Y. Zenitani, and J. Akimitsu , *Nature*, **410**: 63 (2001).
2. C. Buzea and T. Yamashita, *Supercond. Sci. Technol.*, **14**: R115 (2001).
3. V. A. Gasparov, N. S. Sidorov, I. I. Zverkova, and M. P. Kulakov, *JETP Lett.*, **73**: 532 (2001).
4. E. Wuchina, M. Opeka, S. Causey, K. Buesking ,J. Spain, A. Cull, J. Routbort, and F. Guitierrez-Mora, *J. Mater. Sci.*, **39**: 5939 (2004).
5. W. Zagozdzon-Wosik, I. Rusakova, C. Darne, Z. H. Zhang, P. V. D. Heide, and P. Majhi, *J. Microsc.*, **223**: 227 (2006).
6. L. Zhang, D. A. Pejakovic, J. Marschalland, and M. Gasch, *J. Am. Ceram. Soc.*, **94**: 2562 (2011).
7. M. Mallik, A. J. Kailath, K. K. Ray, and R. Mitra, *J. Eur. Ceram. Soc.*, **32**: 2545 (2012).

8. S. N. Dub, A. A. Goncharov, S. S. Ponomarev, V. B. Filippov, G. N. Tolmacheva, and A. V. Agulov, *J. Superhard Mater.*, **33**: 151 (2011).
9. D. Wiley, W. R. Manning, and O. Hunter, *J. Less-Common Met.*, **18**: 149 (1969).
10. J. W. Lawson, C. W. Bauschlicher, and M. S. Daw, *J. Am. Ceram. Soc.*, **94**: 3494 (2011).
11. X. Zhang, X. Luo, J. Han , J. Li, and W. Han, *Comput. Mat. Sci.*, **44**: 411 (2008).
12. E. Deligoz, K. Colakoglu, and Y. O. Ciftci, *Comput. Mat. Sci.*, **47**: 875 (2010).
13. X. Zhang, X. Luo, J. Li, P. Hu, and J. Han, *Scr. Mater.*, **62**: 625 (2010).
14. Y. Yang, S. Jayaraman, B. Sperling, D. Y. Kim, G. S. Girolami, and J. R. Abelson, *J. Vac. Sci. Technol.*, **25**: 200 (2007).
15. P. B. Allen, *Phys. Rev. B*, **6**: 2577 (1972).
16. S. Y. Savrasov and D. Y. Savrasov, *Phys. Rev. B*, **54**: 16470 (1996).
17. J. Perdew and Y. Wang, *Phys. Rev. B*, **45**: 13244 (1992).
18. P. E. Blochl, O. Jepsen, and O. K. Andersen, *Phys. Rev. B*, **49**: 16223 (1994).
19. M. Stuemke and G. Petzow, *Z. Metallkd.*, **66**: 292 (1975).
20. J. P. Perdew, K. Burke, and M. Ernzerhof, *Phys. Rev. Lett.*, **77**: 3865 (1996).
21. P. Ordejon, E. Artacho, and J. M. Soler, *Phys. Rev. B*, **53**: R0441 (1996).
22. O. F. Sankey and D. J. Niklewski, *Phys. Rev. B*, **40**: 3979 (1989).
23. N. Troullier and J. L. Martins, *Phys. Rev. B*, **43**: 1993 (1991).
24. W. L. McMillan, *Phys. Rev. B*, **167**: 331 (1968).
25. Y. S. Tyan, L. E. Toth, and Y. A. Chang, *J. Phys. Chem. Solids*, **30**: 785 (1969).
26. P. B. Allen and R. C. Dynes, *Phys. Rev. B*, **12**: 905 (1975).